ELSEVIER

Polymer 40 (1999) 4195–4203

polymer

The role of metastability in the micromorphologic features of sheared isotactic polypropylene melts

Chang-Mou Wu[a], Ming Chen[a,*], József Karger-Kocsis[b]

[a]*Institute of Materials Science and Engineering, National Sun Yat-Sen University, Kaohsiung, Taiwan 80424, Republic of China*
[b]*Institut für Verbundwerkstoffe GmbH, Universität Kaiserslautern, Pf. 3049, Kaiserslautern D-67653, Germany*

Received 1 July 1998; received in revised form 7 September 1998; accepted 18 September 1998

Abstract

The micromorphologic features of sheared isotactic polypropylene (iPP) in the vicinity of fibre were investigated through polarized light microscopy (PLM), phase contrast optical microscopy (PCLM), scanning electron microscopy (SEM), and atomic force microscopy (AFM). The results indicate that the polymorphic structures and their boundary lines can be explained from a modified model by combining the concept of metastability and the theory of shear-induced crystallization without assuming epitaxial growth. © 1999 Elsevier Science Ltd. All rights reserved.

Keywords: Polypropylene; Crystallization; Sheared melt

1. Introduction

Isotactic polypropylene (iPP) is a polymorphic material with a number of crystal modifications. On the basis of crystal lattice, there are three major crystal forms [1–8]: the α-, the β-, and the γ-forms with monoclinic [1], hexagonal, [2,3] and orthorhombic [4–6] lattices, respectively. Earlier the γ-form [7,8] was identified as a triclinic cell which can be considered as a part of the orthorhombic cell [9]. These polymorphs are all based on 3_1 helices with only the spatial arrangements of the helical chains that are different. The high-temperature monoclinic α form is thermodynamically the most stable crystal form. A metastable β hexagonal form has been reported under special crystallization conditions, such as a thermal gradient, shearing or elongation of the polymer melt during crystallization and nucleating agents in the polymer. The γ-form is preferred in degraded, low molecular weight PP, or in samples crystallized slowly under high pressure.

Based on the results of the thermo-optical studies in the quiescent [10–12] and in the sheared [13–17] PP melts, Varga and Karger-Kocsis [12,17] proposed a schematic diagram to describe the difference between transcrystallization and cylindritic (or shear-induced) crystallization. The former is caused by heterogeneous nucleation in the quiescent melt, whereas the latter is induced by self-nucleation. Owing to the limited resolution of polarized light microscopy (PLM), the micromorphologic features at the fibre/polymer interface cannot be captured. The authors [12,17] explained the formation of this polymorphic structure by assuming that melt-shearing, caused by fibre pulling, is associated with the formation of α-row nuclei. The surface of the in situ formed α-row nuclei may induce the nucleation of the β-form. They believed that auto-epitaxy in iPP may be a possible explanation for the observed α-β bifurcation on the α row-nuclei.

In PP melts sheared by fibre pulling, a polymorphic cylindritic morphology can form around the fibre. The micromorphologic feature was reported as being the α form near the fibre/polymer interface by selective melting of the β-form [14]. At this interface, an overgrowth of the β-form was observed for temperatures $100°C < T_c \leq T_{pull} < 140°C$, where T_c is the crystallization temperature and T_{pull} is the fibre pulling temperature. Varga quantitatively analyzed the boundary lines developed between cylindrite and spherulite [14], spherulite and spherulite [18] by using mathematical equations. Under isothermal conditions, the nucleation may proceed simultaneously or at different times. On the other hand, the β form grows from 20% to 70% faster than the α form between 138°C and 122°C [19]. This permits the observation of characteristics of boundary lines between α-cylindrite and β-spherulites

* Corresponding author. Tel.: +886 7 525 2000 4062; Fax: +886 7 525 4099.
E-mail address: mingchen@mail.nsysu.edu.tw (M. Chen)

PII: S0032-3861(98)00682-X

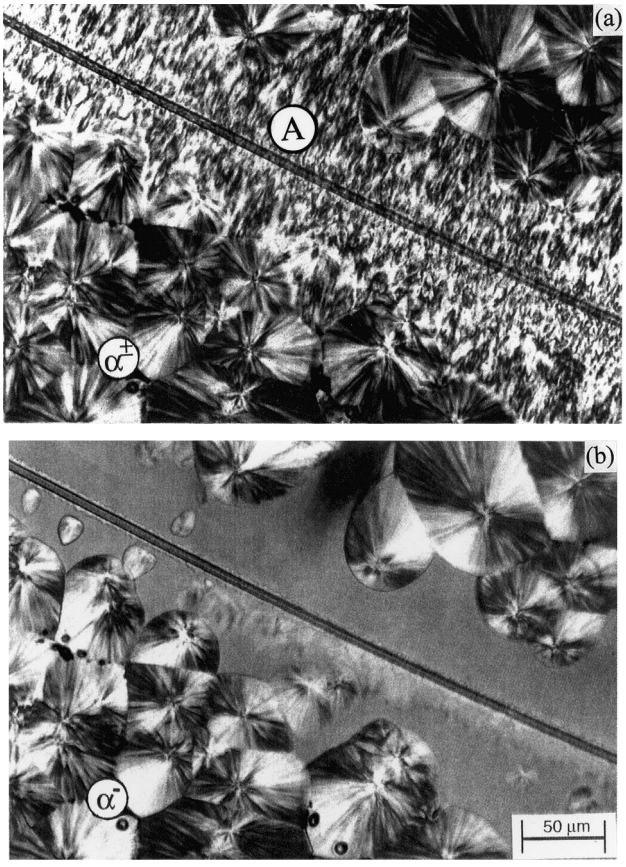

Fig. 1. Cross-polarized optical micrographs of β-cylindrite formation caused by pulling the Kevlar 49 fibre in the crystallizing α-iPP melt under the conditions $T_c = T_{pull} = 133$°C. (a): Polymorphic structures after isothermal crystallization. (A contains both α and β forms); (b): Texture after the selective melting of the β-form at 156°C. Negative radial α-spherulites with parabolic boundary lines are clearly discernible.

nucleated at the same moment, between β-cylindrite and α-spherulites nucleated at different moment, and between α-spherulites nucleated at the same and/or different moments.

In a recent review, Keller and Cheng [20] discussed the role of metastability in the polymer phase and in phase transition behaviors. A classical metastable state may exist because of its fast kinetic pathway even though this state is thermodynamically less stable than the equilibrium state. Another class of metastability is associated with phase size. The authors connected these two categories of metastable states and proposed a possibility ''stability inversion with size.'' Examples of phase inversion with size include polyethylene crystallization and the initial transient states in poly(ethylene oxide) crystallization. Therefore, they suggested classical multiple polymorphs are related with size-dependent morphological metastability.

Kobayashi and Nagasawa [21] investigated the crystallization kinetics of molten polyethylene as a function of temperature at various rates and have derived a set of equations for the sheared polymer melt. According to the theory of rubber elasticity, they accounted for the entropy decrease by molecular orientation. In the high temperature region, both rates of nucleation and growth increase rapidly with molecular orientation. However, they found theoretically and experimentally that the thickness of crystals grown at higher shear rates was thinner in spite of the higher temperature at which crystallization started. Yeh and Hong [22,23] derived two equations for strain induced nucleation based on the reduction in melt entropy. Consequently, the decrease in critical size nucleus and the decrease in free energy required for the formation of a critical nucleus lead to the tremendous increase of nucleation rates in sheared melt. In addition, an equation for the equilibrium melting temperature elevation could also be accounted for by the entropy decrease in sheared melts.

In this contribution, the nature of the cylindritic micromorphologic feature at the iPP-Kevlar 49 interface has been investigated through PLM, phase contrast optical microscopy (PCLM), scanning electron microscopy (SEM), and atomic force microscopy (AFM). Schematic diagrams depicting the polymorphic boundary lines and a schematic plot describing the formation of metastable phase are proposed to explain the origin of the β-cylindrite micromorphologic feature without the assumption of epitaxial crystallization. Finally, the effect of high temperature pulling on the cylindritic polymorphism will be discussed.

2. Experimental

The α-iPP resin used in this study was a Novolen 1100N grade, marketed by BASF (Germany). The β-iPP resin was a Daplen BE 50 821c grade, marketed by PCD (Linz, Austria). An Aramid fibre (Kevlar 49, DuPont, USA) was placed in an iPP film between two glasses which resulted in a thickness of about 30–50 μm. PLM investigations were carried out in a Leitz Dialux 20 microscope, equipped with a hot stage. The specimens were heated to 200°C and maintained at this molten state for 5 min. The hot stage was then cooled to the crystallization temperature ($T_c = 133$°C) at a rate of 40°C/min. The fibre was manually pulled at T_c and the specimens were allowed to crystallize for 1 h. The optical character, i.e., the sign of birefringence of the micromorphologic feature was determined by means of a primary red filter (λ-plate) located diagonally between cross polarizers. The course of crystallization was followed by taking color pictures. In this way the first and third quarters of the sight were yellow and the second and fourth were blue when the forms were negative, while a reversed arrangement of the quarters were observed for positive forms. Black-and-white copies of these colored pictures after treatment through a scanner and software are presented in this contribution representing the yellow and blue fields by lighter and darker tints, respectively.

These specimens were later etched chemically according to the procedure of Olley et al. [24] in order to study the interface morphology by PCLM (Leitz, Wetzlar, Germany), AFM, and SEM (JEOL 6400). AFM experiments were

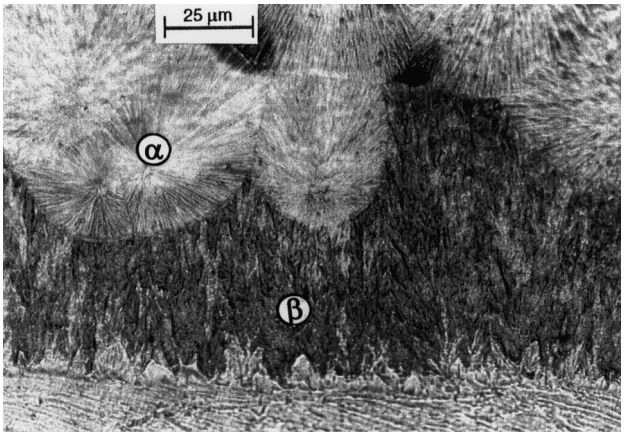

Fig. 2. Phase contrast optical micrograph after chemical etching of α-iPP with β-cylindrite formed by pulling a Kevlar 49 fibre under the conditions $T_c = T_{pull} = 133$°C. The fibre/polymer interface is located below the bottom margin of the micrograph.

performed in air at room temperature in a tapping mode by using a MultiMode scanning probe microscopy manufactured by Digital Instruments, Santa Barbara, CA, USA. A microfabricated silicon cantilever with an integral tip (tapping mode tip) was used to examine the surface topology of polymorphism in the vicinity of fibre after chemical etching. Two AFM imaging modes can be adopted in the tapping mode: the height mode, and the amplitude mode which is obtained from the error signal of the feedback loop. An amplitude image is equivalent to a first derivative of the height image which provides a real topographic image. The scanning frequency was 0.6 Hz and all images shown were captured without the use of image filtering. In addition, four high temperatures shearing at 160°C, 165°C, 168°C or 170°C, respectively, and subsequent static crystallization at 133°C without any further displacement of the fibre were applied to α-iPP in a hot stage, the cylindritic polymorphism was then observed under PLM only.

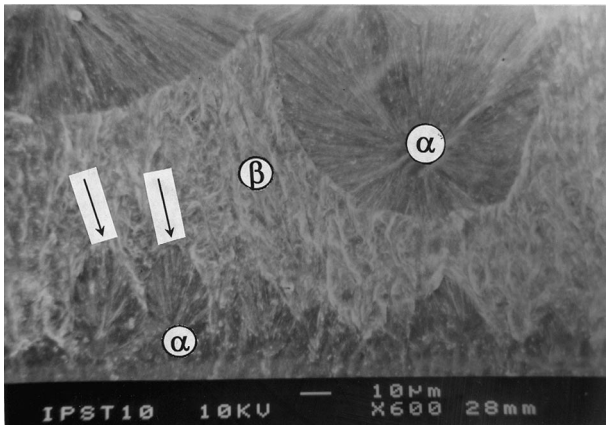

Fig. 3. Scanning electron micrograph after chemical etching of α-iPP crystallized isothermally at $T_c = T_{pull} = 133$°C. The α- and β- cylindrites with palm shape boundary are clearly discernible. The fibre-polymer interface is located below the bottom margin of the micrograph.

3. Results

3.1. Micromorphologic feature in sheared α-iPP melt

The PLM micrograph consisting of cylindrites and α-spherulites is shown in Fig. 1a where symbol A shows a mixed polymorphic structure ($\alpha + \beta$). α-spherulites appeared in the sample (generally at a considerable delay and 20–60 μm from the fibre) with a mixed birefringence. The β-form in the specimen was selectively melted out during heating from T_c to 156°C, only the α-crystalline region remained in the form of spherulites and a sawtooth-like pattern around the fibre is clearly visible in Fig. 1b. It is clear in the pictures by inspecting the lighter and darker tints in the quarters that the mixed α-spherulites (with lighter and darker strips alternate irregularly) transform into α-negative ones. In addition, negative α-spherulites exhibit a clear Maltese cross. The shape of the boundary between the α-spherulites and the β-cylindrite was particularly conspicuous as the β-modifications had completely fused. The boundary line between the β-cylindrite and the α-spherulite was ellipsoidal. Because of the greater growth rate of the β-form with regard to the α-form, the former crystal developed in the shape of cylindrite which would lead a bulk α spherulite to develop in a teardrop shape. The boundary line between each pair of α-spherulites was straight or hyperbolic. This particular geometry confirms the various crystallographic natures of the two forms present.

Fig. 2 depicts the morphology after chemical etching revealed by PCLM which shows a clearly interfacial shear zone (pre-oriented crystalline zone near the bottom edge), α-cylindritic layer, β-cylindritic layer and α-spherulites. The β-cylindritic layer is about a few μm to 10 μm distant from the interfacial shear zone containing oriented polymer chains along the fibre length. As shown in the SEM micrograph (Fig. 3), an α-cylindritic layer with palm shape (arrows) is formed with a distance of about 20 μm between two point-like β-nuclei which are not located on the surface of the pre-oriented crystalline zone. Because of the greater growth rate of the β-form (G_β) with regard to the α-form (G_α), the β-cylindritic growth terminated the growth of the primary α-cylindritic front and produced an α-cylindrite to be developed in a palm shape. Both micrographs indicate that the impingement lines between α- and β-cylindritic layers are not completely straight.

Fig. 4 displays $(60\ \mu m)^2$ scan: Fig. 4a displays the amplitude mode, and Fig. 4b shows the surface plot. In both cases the fibre is located near the left margin of the micrographs (the fibre itself is not shown). The basic morphological features observed in AFM images are similar to the images obtained by SEM: the point-like β-nucleus in the vicinity of fibre is obvious and the β-cylindritic structure can be clearly seen. Fig. 4b shows a perspective, quasi-three dimensional surface plot of the α- and β-cylindritic morphology. The vertical scale in this picture corresponds to 2.8 μm per

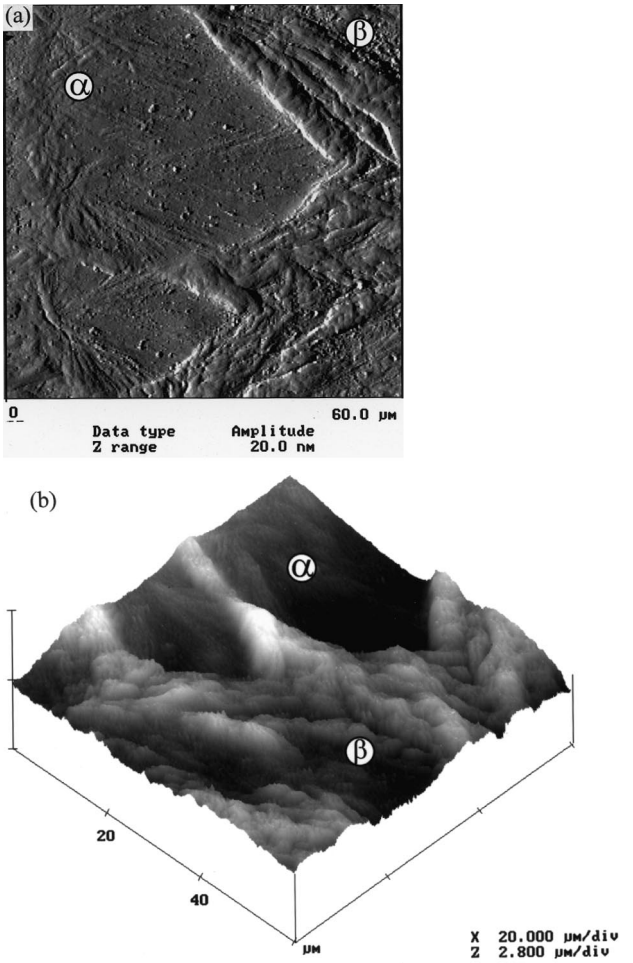

Fig. 4. AFM micrographs (image size: 60 μm × 60 μm) of the etched α-iPP specimen with β-cylindrite formed by pulling the Kevlar 49 fibre at $T_{pull} = T_c = 133$°C. (a): Amplitude image; (b): Surface plot showing true ''three-dimensional'' topology of the α-form inclusion in β-cylindritic morphology.

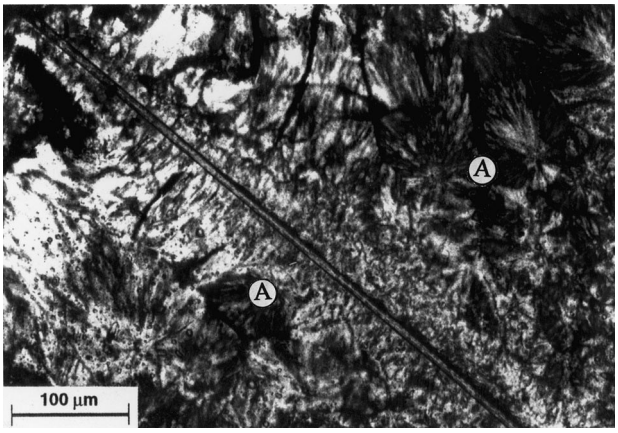

Fig. 5. Cross-polarized optical micrograph of the shear-induced crystallization of β-nucleated iPP by pulling the Kevlar 49 fibre at $T_c = T_{pull} = 133$°C. The thickness of β-cylindrite increases along the pulled direction from the left-top corner to the right-bottom corner. (A contains both α and β forms.)

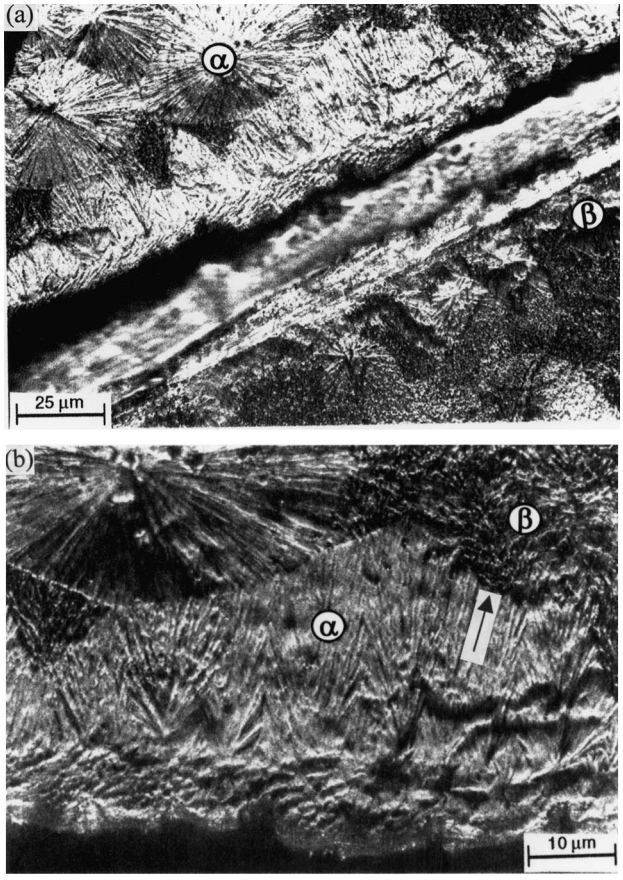

Fig. 6. (a): Phase contrast optical micrograph after chemical etching of β-iPP with β-cylindrite formed by pulling a Kevlar 49 fibre under the conditions $T_c = T_{pull} = 133$°C; (b): A close-up of α-cylindrite texture. The fibre-polymer interface is located below the bottom margin of the micrograph.

division (as opposed to the 20 μm per division for the horizontal x and y axes), i.e., the surface morphological features are emphasized in the vertical direction. Near the left edge, an α-cylindrite is seen. The boundary lines between the α- and β-cylindrites are not straight in the centre of the micrograph. Although a thickness difference between the α- and β-forms may be found, it is difficult to explain this observation. Is the thickness difference truly a representation of the difference in lamellar crystal thickness? If it is, the lamellar thickness of the metastable β-form has to be larger than that of the stable α-form. The elucidation of this phenomenon is the focus of our ongoing research.

3.2. Micromorphologic feature in sheared β-iPP melt

The PLM micrograph in Fig. 5 exhibits the basic feature of shear induced cylindritic morphology in β-iPP. In this case the fibre was pulled for a short distance. The thickness of the β-cylindritic zone along the fibre increases slightly from the left-top corner to the right-bottom corner. Based on the morphology in Fig. 5, one can conclude that the size of the β-cylindrite depends on the intensity of shearing. In

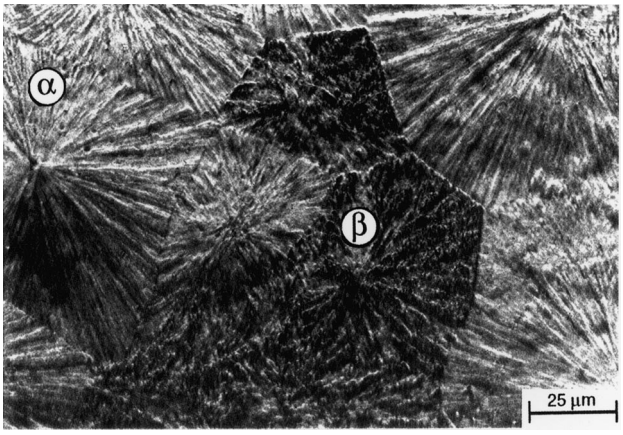

Fig. 7. Phase contrast optical micrograph after chemical etching of β-iPP crystallized isothermally at $T_c = T_{pull} = 133$°C. In the quiescent area, the β hexagonal form grew in the field of α-spherulites.

addition to the cylindrite the sample contains a great density of α- and β-modification crystals, which results in distorted boundaries between the α- and β-forms [25].

Figs. 6a,b depict the morphology after chemical etching revealed by PCLM which elucidates the α-cylindritic layer, β-cylindritic layer, α-spherulites, and a clearly pre-oriented crystalline zone on both sides of the pulled fibre. A close-up of α-cylindrite texture on the left side of fibre is shown in Fig. 6b. The number (or the density) of point-like or fibril type α-nuclei at 10–20 μm distant from the shear zone is larger compared with the only one nuclei in an α-spherulite. Thus α cylindrite formation is favored in the close vicinity of the fibre. The boundary lines between α-cylindrite and β-spherulites (later developed into β-cylindrite) are hyperbolic, as shown in the right part of Fig. 6b (arrow). The boundary line between α-cylindrite and α-spherulite is parabolic (see Figs. 6a,b). In the left-top corner of Fig. 6a, straight or hyperbolic lines are observed between each pair of α-spherulites. In the area far distant from the pulled fibre, nucleation of the α- and β forms is observed sporadically in the crystallization of quiescent melts as shown in Fig. 7. The random appearance of the hexagonal form of β-modification was detected in addition to the mixed α-spherulites in the presence of β-nucleating agents.

The SEM micrographs in Figs. 8a,b show a clearly pre-oriented crystalline zone near the bottom side of the pulled fibre. The α-cylindritic layer, in a sawtooth-like shape, is located between the pre-oriented crystalline zone and β-cylindritic layer. However, the boundary lines between α-cylindrite and β-spherulites (later developed into β-cylindrite) are not completely straight, which indicates some of the point-like β-nuclei are not located on the surface of the pre-oriented crystalline zone. The column-like β-cylindrite and the impingement line (β-β) are clearly visible in Fig. 8a, then the boundary line between β-cylindrite and α-spherulites becomes ellipsoidal. Fig. 9 shows a scan depicting a $(60\ \mu m)^2$ area near the fibre which is located at the right-bottom edge. Some of the boundary lines between α- and β-cylindrites are not straight, thus the inclusions of the α-form within the polymorphous cylindrite are not completely trianglar.

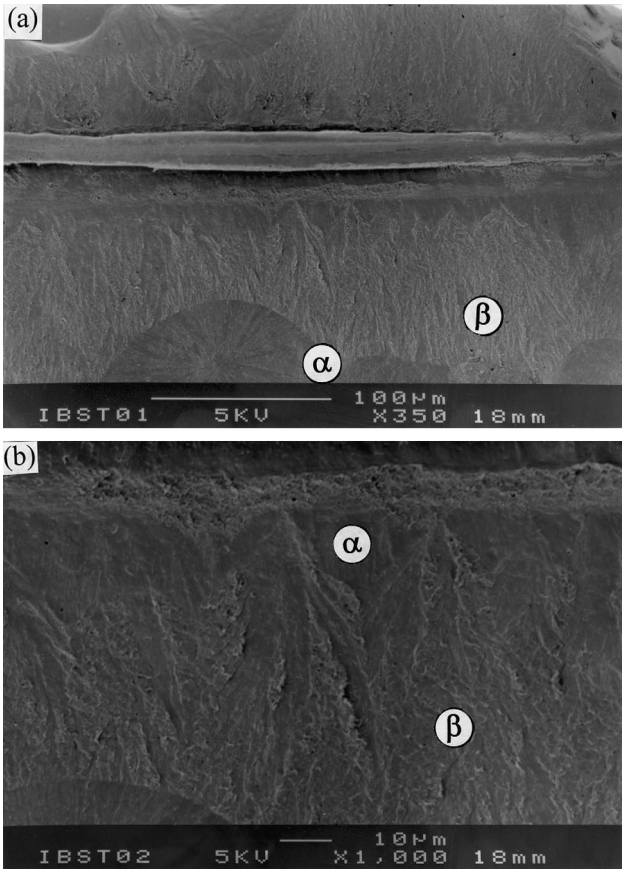

Fig. 8. (a): Scanning electron micrograph of the etched cylindritic region in β-iPP caused by pulling a Kevlar 49 fibre under the conditions $T_c = T_{pull} = 133$°C; (b): A close-up of α- and β-cylindrites formed near the surface of the Kevlar 49 fibre. The fibre-polymer interface is located above the top margin of the micrograph.

4. Discussion

4.1. Shear-induced crystallization

The results of previous works [11,12] indicated that only α-form was observed in quiescent α-iPP melts, which demonstrated $N_\alpha \gg N_\beta$, where N is the number of nuclei. In melts sheared by fibre pulling, the point-like β-nuclei were reported near the interface for both α- and β-iPP. An overgrowth of the β-form was observed for temperatures $100°C < T_c \leq T_{pull} < 140°C$, where $G_\beta > G_\alpha$ and $N_\alpha > N_\beta$. The stresses produce molecular orientation along the direction in which the fibre is pulled, and thus cause a reduction in entropy. The difference in entropy between oriented melt and crystal is raised with respect to that in quiescent melt. Yeh and Hong [22] estimated that the tremendous increase of nucleation rates in sheared polyethylene melt can be several orders of magnitude higher than that in the

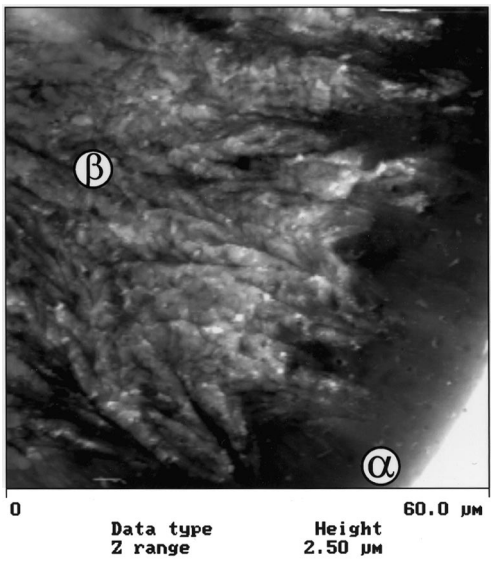

Fig. 9. AFM image of the etched cylindritic region in β-iPP caused by pulling a Kevlar 49 fibre under the conditions $T_c = T_{pull} = 133°C$. Scan size: 60 μm × 60 μm.

quiescent state if the nucleation is heterogeneous, and the enhancement in homogeneous nucleation is much higher. It should be noticed that there are β heterogeneous nuclei in β-iPP melts. By pulling a fibre, the induced crystallization near the interface starts earlier than for the heterogeneous or homogeneous ones. The earlier stage of formation of the β-cylindritic layer inhibits the growth of β heterogenerous and α homogeneous nuclei. This shear-induced crystallization is located only on the fibre surface as a result of the strong decrease of shear stresses along the radius [26]. It should be emphasized that increasing shear force involves increasing growth rates (G_α and G_β) simultaneously with increasing the relative number of β-nuclei, as well as the size of cylindrite (see Fig. 5). In addition, this enhances the melting temperature and the degree of supercooling.

4.2. Shape of cylindrite–spherulite and spherulite–spherulite boundaries

Varga [14] described the boundary lines of cylindrite–spherulite by using mathematical equations. He defines ''d'' as a distance from the surface of the cylindrite to the nucleus of the spherulite, ''t_o'' as positive if growth of the spherulite starts later than that of the cylindrite. Growth rates of the spherulite and the cylindrite are designated with G_s and G_c, respectively, and the relative growth rate with G_r ($= G_s/G_c$). If $d < G_c t_o$, the nucleus of the spherulite is absorbed by the growing cylindritic front, and if $d < -G_s t_o$ then a definite section of the cylindritic nucleus is absorbed by the spherulite. The boundary lines are hyperbolic shape if $d > 0$ and $G_r > 1$, straight lines if $d = 0$ and $G_r > 1$, or ellipsoidal shape if $d > 0$ and $G_r < 1$.

It should be noted that (a) the growth rate of the β form is about 30% faster than that of the α form at 133°C when crystallized from quiescent melts [19], i.e., $G_\beta/G_\alpha \approx 1.3$, and (b) the crystallization of sheared melts occurs earlier and faster than that in quiescent melts [21]. The relationship of $G_\beta/G_\alpha > 1$ still exists at 133°C. In sheared iPP melts the pre-oriented crystalline zone is formed first and $N_\alpha > N_\beta$ in the vicinity of pulled fibre. A great number of α nuclei develop into α-cylindrite and the point-like β nuclei grow radially. The boundary lines between α-cylindrite and β-spherulites are hyperbolic because $G_r (= G_s/G_c = G_\beta/G_\alpha) > 1$. Straight-line boundaries may also be formed if β-nuclei are sporadically initiated on the growing α-cylindritic front, i.e., $d = 0$ or $d \to 0$. The β-spherulite growing at a higher rate will encompass the α-cylindrite, which thus becomes an inclusion. During the formation of an inclusion, the growing fronts of the β-spherulite meet behind the inclusion forming a straight intrinsic $\beta\beta$-spherulitic boundary, which leads to the characteristically micromorphologic feature of β-cylindrite. The formation of α-ellipsoidal inclusions surrounded by β-cylindrite is observed as a result of the time lag of nucleation of α-form with the lower growth rate as shown in Fig. 1b. Finally, the front of β-cylindrite meets with α-spherulites which are sporadically initiated in quiescent melts. In this case of G_r ($= G_s/G_c = G_\alpha/G_\beta$) < 1, the boundary lines are ellipsoidal. Spherulites growing at the same rate form hyperbolic ($V_r = 1$ and $t_o \neq 0$) or straight line ($V_r = 1$ and $t_o = 0$) boundaries. If two nuclei grow at different rates ($V_r \neq 1$), the boundary line between them will be circular if $t_o = 0$.

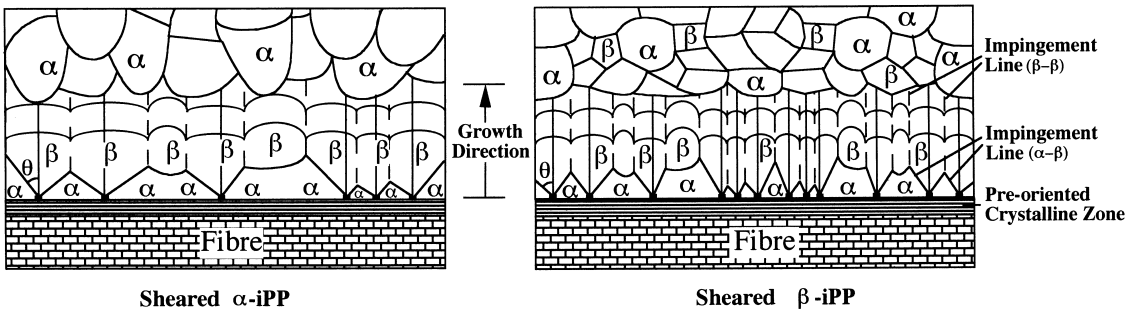

Fig. 10. Schematic diagrams of the difference of the shear-induced crystallization between α-iPP and β-iPP under the conditions: $T_c = T_{pull} = 133°C$ and $G_\beta/G_\alpha \approx 1.3$.

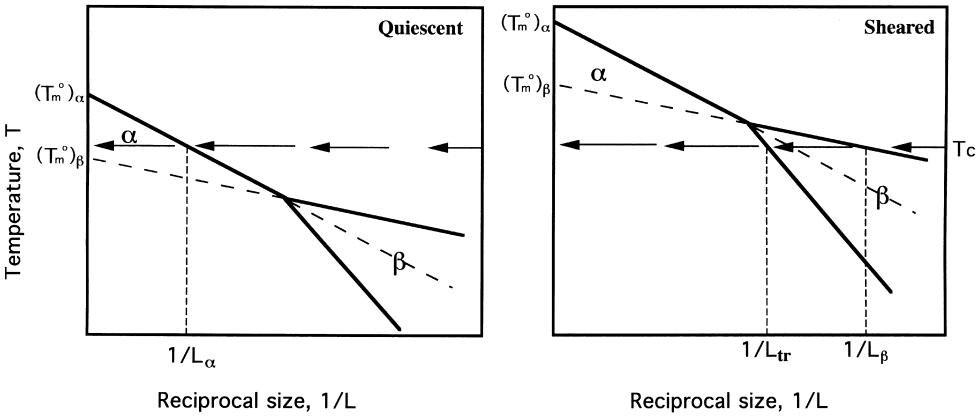

Fig. 11. Crystal growth as temperature versus reciprocal size, $1/L$. (→) Pointing denotes isothermal growth pathways at the selected crystallization temperature, T_c. Two condition are indicated, one quiescent melt and one sheared melt. $(T_m^o)_\alpha$ and $(T_m^o)_\beta$ are the equilibrium melting temperature of α- and β-forms, respectively.

In Figs. 2–4 and Figs. 6–9, we show the interfacial region near the fibre-melt interface with a magnification significantly higher than the resolution limit of optical microscopy. These micrographs yield valuable information regarding the micromorphologic feature of sheared melts in the vicinity of fibre. Combining the theory of stress-induced crystallization [21–23] and the mathematical equations of the boundary lines [14,18], from Fig. 10 we propose a modified model to depict the shape of boundary lines in sheared α- and β-iPP melts. The shape of the boundary between α-cylindrite and β-spherulites depends on the distance between α-cylindrite and point-like β-nuclei, the distance between point-like β-nuclei, and on the absolute and relative growth rates of α- and β-forms. In addition, the experimentally observed shape of inclusions boundary differs from that expected from the above model because the density of β-nuclei depends on the applied stress [27], the pulling temperature, and the crystallization temperature. This modified model can depict the micromorphologic features without assuming epitaxial growth. It is therefore important to determine the β-cylindritic crystallization mechanism.

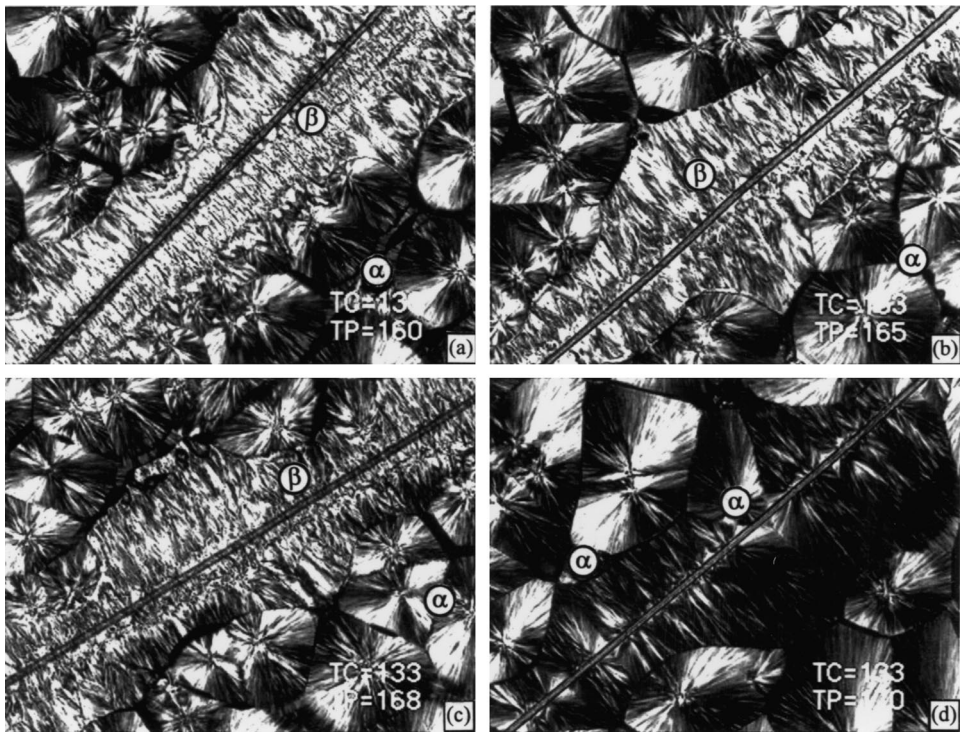

Fig. 12. Effect of fibre-pulling temperature on the formation of the β- or α-cylindritic morphology, respectively. (a): 160°C; (b): 165°C; (c): 168°C; (d): 170°C.

4.3. The role of metastability

Based on the observation that $G_\beta/G_\alpha \approx 1.3$ at 133°C in the quiescent state [19], only a relative small number of β-nuclei in the vicinity of the pre-oriented crystalline zone is necessary to produce a β-cylindrite structure. Kobayashi and Nagasawa [21] found theoretically and experimentally that the thickness of crystals grown at higher shear rates were thinner in spite of the higher temperature at which crystallization starts. This result is contrary to the usual expectation of thicker crystals at higher crystallization temperature, but supports the concept of metastability [20] in which the classical metastable state can become the stable one when phase dimensions are small enough.

For making a comparison on a reciprocal scale of the lamellar thickness ($1/L$), the crystallization always occurs directly to the stable state, as shown in Fig. 11. In view of the fact that $(T_m^o)_\beta nf < (T_m^o)_\alpha$, the T_m versus $1/L$ lines are promoted simultaneously under sheared condition. As described in the previous section on shear induced crystallization, Fig. 11 provides a schematic plot that the metastable phase possesses higher stability at its initially small size and grows at a faster rate in the sheared melt. Therefore, the metastable phase will dominate the crystallization with its more rapidly increasing rates. This results in the overgrowth and inclusion of the stable phase. The conception of stability inversion becomes readily applicable to iPP if the phases to be refereed to as stable and metastable are taken, respectively, as the α and β forms. The origin of a metastable β-form is being accounted for kinetically through the smaller energy barriers involved in its formation. On this basis, the origin and the boundary shape of the β-cylindrite (or the phenomenon of polymorphic structure of sheared PP melt in the vicinity of a pulling fibre) can be interpreted by both shear-induced crystallization theory and the metastability concept.

The recent metastability model is an alternative explanation to the earlier proposed one [12,17] in which the driving force was traced to auto-epitaxy. Further investigations are needed, however, to conclude which one of them is more straightforward and reflects the realty accordingly.

4.4. Effect of fibre-pulling temperature

Figs. 12a–d show the micrographs after fibre shearing of a molten α-iPP at high temperatures and the subsequent isothermal crystallization ($T_c = 133$°C) under static condition. The sheared melt has lost its β crystallization ability as a result of the thermal treatment at $T_{pull} = 170$°C (see Fig. 12d). The viscosity of the melt at higher T_{pull} is reduced so that the shear stress strongly decreases. A critical threshold of shear stress [27] cannot be exceeded at $T_{pull} = 170$°C, and the crystallization follows the pathway as shown in the left part of Fig. 11. The other possible reason is polymer relaxation during fibre pulling and during cooling to the crystallization temperature. The hyperbolic and straight lines along the boundary lines of cylindrite and spherulites in Fig. 12d clearly demonstrate that α-cylindrite occurred in the melt. The α-cylindrite becomes even more obvious if one views the bright appearance of the β-cylindrite present in Figs. 12a–c.

5. Conclusion

The results presented here show that shear at the polymer/matrix interface promotes the orientation of the polymer chains in the stress direction, which results in a pre-oriented crystalline zone. The polymorphic structure and the boundary lines of sheared α- and β-iPP melt in the vicinity of pulled fibre can be explained from a modified model by combining the concept of metastability and the theory of stress-induced crystallization without assuming epitaxial growth.

Acknowledgements

C.-M. Wu is thankful for the fellowship at the IVW in Kaiserslautern granted by the DAAD. It is a pleasure to acknowledge the valuable review manuscript from Professor Stephen Z. D. Cheng at The Maurice Morton Institute and Department of Polymer Science, The University of Akron. Part of this work was financially supported by the National Science Council, ROC, under contract number NSC 87-2216-E110-011.

References

[1] Natta G, Corradini P. Nuovo Cimento Suppl 1960;15:40.
[2] Turner-Jones A, Cobbold AJ. J Polym Sci 1968;B6:539.
[3] Samuels RJ, Yee RY. J Polym Sci A-2 1972;10:385.
[4] Bruckner S, Meille SV. Nature 1989;340:455.
[5] Meille SV, Bruckner S, Porzio W. Macromolecules 1990;23:4114.
[6] Lotz B, Graff S, Straupe C, Wittmann JC. Polymer 1991;32:2902.
[7] Turner-Jones A, Aizlewood ZM, Beckett DR. Makromol Chem 1964;75:134.
[8] Morrow DR, Newman BA. J Appl Phys 1968;39:4944.
[9] Kressler J. in: Krager-Kocsis J, editor. Polypropylene: An A–Z reference, London: Chapman and Hall, 1998. pp. 267.
[10] Varga J, Karger-Kocsis J. Polym Bull 1993;31:707.
[11] Varga J, Karger-Kocsis J. J Mater Sci Lett 1994;13:1069.
[12] Varga J, Karger-Kocsis J. Polymer 1995;36:4877.
[13] Leugering HJ, Kirsch G. Angew Makromol Chem 1973;33:17.
[14] Varga J. Angew Makromol Chem 1983;112:191.
[15] Varga J, Karger-Kocsis J. Polym Bull 1993;30:105.
[16] Varga J, Karger-Kocsis J. Compos Sci Technol 1993;48:191.
[17] Varga J, Karger-Kocsis J. J Polym Sci Part B: Polym Phys 1996;34:657.
[18] Varga J. J Mater Sci 1992;27:2557.
[19] Lovinger AJ, Chua JO, Gryte CC. J Polym Sci Polym Phys Edn 1977;15:641.
[20] Keller A, Cheng SZD. Polymer 1998;39:4461.
[21] Kobayashi K, Nagasawa T. J Macromol Sci-Phys 1970;B4:331.

[22] Yeh GSY, Hong KZ. Polym Eng Sci 1979;19:395.
[23] Yeh GSY, Hong KZ, Krueger DL. Polym Eng Sci 1979;19:401.
[24] Olley RH, Bassett DC. Polymer 1982;23:1707.
[25] Wu C-M, Chen M, Karger-Kocsis J. Polym Prep 1998; 39(2) (in press).
[26] Monasse B. J Mater Sci 1992;27:6047.
[27] Dragaun H, Hubeny H, Muschik H. J Polym Sci Polym Phys Edn 1977;15:1779.